A New Ultraminiaturized Low-profile and Stable FSS with 2.5D Structure for 900 MHz ISM Band

Mychael J. Duarte, Adaildo G. D'Assunção Jr, Valdemir P. Silva Neto and Adaildo G. D'Assunção

***Abstract*— This paper presents a new 2.5D ultraminiaturized frequency selective surface (FSS) structure to operate in the 900 MHz ISM band (902 to 928 MHz), for application in the Wi-Fi HaLow. The proposed FSS simulation and design are performed using ANSYS HFSS software and equivalent circuit model (ECM). The development of the proposed 2.5D FSS is based on meander-line-based conducting patches and has required the simulation and design of typical (2D) and 2.5D structures. An equivalent circuit model was proposed and presented very accurate results. The cell size of the 2.5D FSS of the proposed cell is only $0.03\lambda_0 \times 0.03\lambda_0$, where λ_0 corresponds to the free space wavelength for the FSS resonant frequency. The FSS presents angular stability for angles up to 50° and its simulated response presented resonant frequencies at 920 MHz, with relative bandwidth of 9.0 %. For comparison purpose, a prototype is fabricated and measured. Good agreement is observed between simulation and measurement results.**

***Index Terms*— Frequency selective surfaces, ultraminiaturized FSS, 2.5D FSS, ISM Band, angular stability, Wi-Fi HaLow.**

I. Introduction

FREQUENCY selective surfaces (FSSs) are spatial filters of electromagnetic waves and, usually, they are composed of periodic arrays of metallic patches printed on dielectric substrates or apertures perforated on very thin conducting sheets [1]-[4]. Basically, the FSSs frequency responses depend on the dielectric substrate properties, array element geometry and shape, array periodicity and electromagnetic wave incidence angle [5]-[7].

The 2.5D (2.5 dimensions) FSS structures have been analyzed and shown to be able to miniaturize the array element dimensions. These FSS structures are composed of two or more layers interconnected by metallic vias throughout the dielectric layers, composing the so called 2.5D structure [8]-[11]. Also, it has been emphasized that these structures provide miniaturization of the array elements with little decrease in the relative bandwidth and without the appearance of new resonance bands [12]-[14].

In [12], the authors have presented a miniaturized and dual-band 2.5D FSS. The proposed application is for the 900 MHz and 1790 MHz GSM band. The unit cells dimensions are $0.072\lambda_0$ x $0.072\lambda_0$.

The main objective of this work is to propose a new 2.5D ultraminiaturized FSS structure to operate in the 900 MHz ISM band (902 to 928 MHz), for possible application in the Wi-Fi HaLow [15].

The developed 2.5D ultra-miniaturized FSS structure is based on meander-line-based conducting patch elements, printed on the top and bottom sides of dielectric substrates, which are interconnected by metallic vias, as described in section II. Analyses of this FSS structure are performed using both ANSYS HFSS software and the equivalent circuit model (ECM).

In addition, a prototype was fabricated and measured, enabling to observe a good agreement between simulated and measured results.

II. FSS Unit Cell and Structure

Fig. 1 shows the design of this surface, its main parameters are: $a_x = a_y = 10.0$ mm, $L_x = 9.1$ mm, $L_y = 8.6$ mm, $L_1 = 2.3$ mm, $L_2 = 1.4$ mm, $D = 0.3$ mm, $R_{via} = 0.15$ mm and $w = 0.6$ mm. The unit cell size is $0.03\lambda_0$ x $0.03\lambda_0$, where λ_0 is the free space wavelength for the FSS resonant frequency. The meander-shaped conductive patches dimensions are also indicated. The dielectric substrate is FR-4 with $\varepsilon_r = 4.4$, $\tan\delta = 0.02$ and $h = 1.57$ mm.

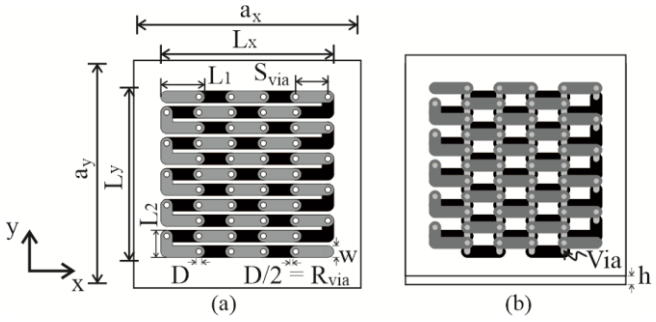

Fig. 1. Geometry of the proposed 2.5D FSS unit cell. (a) Top view and (b) perspective view. Conducting patches at the top side are in grey color and at the bottom side are in black color.

M. J. Duarte, V. P. Silva Neto, and A. G. D'Assunção are with the Federal University of Rio Grande do Norte, 59078-970 Natal, RN, Brazil. (e-mail: adaildo@ct.ufrn.br).

A. G. D'Assunção Junior is with the Federal Institute of Paraíba (IFPB), João Pessoa, PB, Brazil.

This work was supported in part by the National Council for Scientific and Technological Development (CNPq), under covenant 573939/2008-0 (INCT-CSF), and CAPES.

Digital Object Identifier 10.14209/jcis.2023.2

Fig. 2 illustrates the steps for obtaining the unit cell geometry shown in Fig. 1. In Fig. 2(a), an FSS (2D) structure is investigated, which is composed of a meander-line-based conducting patch element printed on the top side of the dielectric substrate.

Then, the unit cell meander-line-based conducting patch element is divided into two parts, left and right sides, as shown in Fig. 2(b). In this case, the left side conducting patches (in black color) are printed on the bottom side of the dielectric substrate and the right side conducting patches (in grey color) are printed on the top side. To provide the FSS ultra miniaturization, several metallic vias are used to successively interconnect the divided conducting patch elements printed on both sides of the dielectric substrate, generating the 2.5D FSS unit cell shown in Fig. 2(b).

In Fig. 2(c), the unit cell meander-line-based conducting patch element is divided into four parts and a similar procedure is used to successively interconnect the divided conducting patch elements. In Fig. 2(d), the FSS unit cell is divided into five parts, generating the proposed 2.5D FSS unit cell shown in Fig. 1.

In Fig. 2, the numbers of interconnecting conducting vias are: (a) 0 (Case 1), (b) 11 (Case 2), (c) 33 (Case 3) and (d) 54 (Case 4).

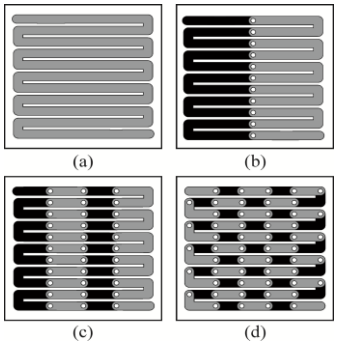

Fig. 2. FSSs conducting patch element designs. (a) Case 1: Meander line at the top side. (b) Case 2: Two parts meander line interconnected by vias. (c) Case 3: Four parts meander line interconnected by vias. (d) Case 4: Five parts meander line interconnected by vias. Conducting patches at the FSSs top side are in grey color and at the bottom side are in black color.

III. Simulated Results

The ANSYS HFSS software was used in the simulation of the proposed FSS structures. The simulations were carried out using periodic boundary conditions, for incidence of electromagnetic waves in the z direction and with TE and TM polarization. The bandwidth in this work was set to -10 dB.

The transmission coefficient simulation results for the FSS geometries presented in Fig. 2 are shown in Fig. 3 for incident electromagnetic waves with TE polarization. In case 1, the structure resonates at 2.54 GHz and 18% relative bandwidth. In case 2, the resonance frequency is 1.9 GHz with 16.5% of bandwidth. In case 3, the resonance is at 1.45 GHz and relative bandwidth equal to 14.5%. In case 4, the FSS structure resonates at 0.92 GHz and 12% relative bandwidth.

As observed in Fig. 3, the proposed 2.5D FSS geometry (Case 4), with the unit cell shown in Fig. 2(d), meets the frequency and bandwidth specifications for application as a stopband filter at the 900 MHz ISM band.

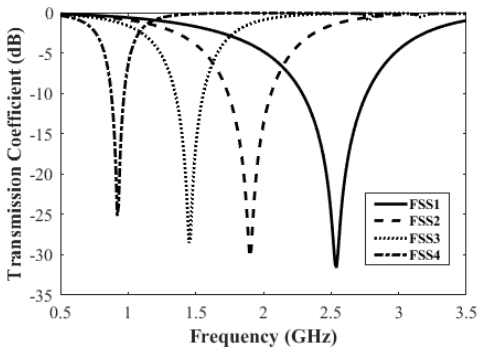

Fig. 3. FSS structures simulated transmission coefficient results for FSS1 to FSS4 illustrated in Figs. 2(a) to 2(d), respectively.

The FSS4 simulated results for the transmission and reflection coefficients are shown in Fig. 4, for both TE and TM polarizations. As can be seen, the structure presents a very good performance for TE polarization and does not present another resonance frequency within the analyzed range. For TM polarization, the FSS4 structure does not exhibit any resonance within the analyzed range.

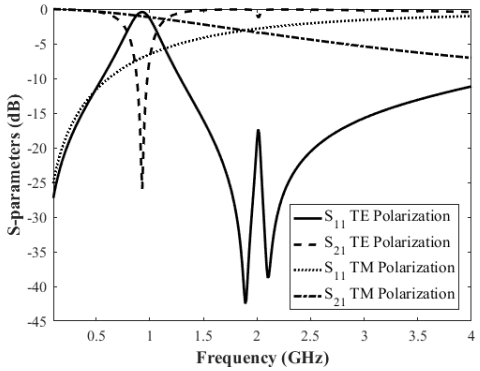

Fig. 4. Simulated transmission and reflection coefficients of the proposed 2.5D FSS illustrated in Fig. 1(a).

In addition, the angular stability of the proposed 2.5D FSS (Case 4) was analyzed. The transmission coefficient simulation results are shown in Fig. 5 at incident angles of 0° (normal to the FSS array), 30° and 50°. Results are for TE polarization. An excellent angular stability is observed. In fact, the FSS resonant frequency is about the same for incident angles up to 50°. Also, bandwidth increases slightly with the increasing of the incident wave angle, preserving the FSS rejection band for incident angles up to 50 °.

IV. Equivalent Circuit Model

In this section, an equivalent circuit model is proposed to better understand the operating principle of the FSS analyzed in the previous sections. The analysis begins by understanding that the proposed element has planar (2D) parts and 2.5D parts, each of these parts contributes inductances and capacitances from which an equivalent circuit can be obtained. The 2.5D parts consist of the vias and the planar parts are the upper and lower metal strips, as can be seen in Fig. 6.

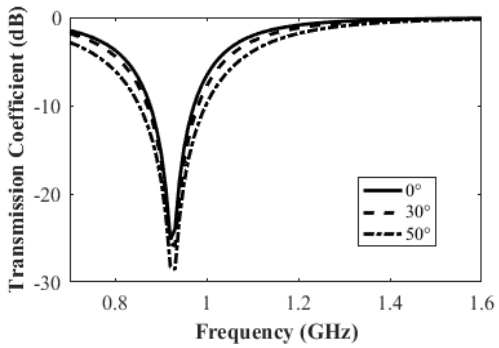

Fig. 5. Simulated transmission coefficients of the proposed 2.5D FSS illustrated in Fig. 1(a), for different angles of electromagnetic wave incidence (0°, 30°, and 50°) with TE polarization.

Fig. 6 shows that the equivalent circuit is composed of a substrate impedance (Z_{sub}), an equivalent inductance (L_{eq}) and an equivalent capacitance (C_{eq}) in series. The inductances L_v and L_t in series and the capacitances C_v and C_t in parallel form the equivalent inductance and the equivalent capacitance, respectively.

The calculated results for L_t and C_t were neglected due to their very very small values. The vias in the FSS elements can be modeled by small L_v inductors and C_v capacitors. These capacitances and inductances can be approximated by the following equations [16].

$$C_v = \frac{\pi \varepsilon_r \varepsilon_0}{\cosh^{-1}(g_{via} / 2R_{via})} \times h \quad (1)$$

$$L_v = \frac{\mu_0}{\pi} \cosh^{-1}(g_{via} / 2R_{via}) \times h \quad (2)$$

Where g_{via} is the distance from the center of one via to the center of the other via.

The capacitance obtained in (1) is the calculation only for a pair of vias, as the structures present arrays of vias, that is, in addition to the pair of vias, there are other nearby vias that influence their distribution of electric field, that is, its capacitance. In [17] an empirical equation was proposed to estimate the total coupling capacitance between adjacent elements of a FSS. This equation is described below.

$$C_{eq} = \alpha C_v (0.6788 \times (N_{via} - 2) + 1.4374) \quad (3)$$

Where N_{via} is the number of vias of the FSS unit cell, α is a correction factor of the per [17]

$$\alpha = \frac{cosh^{-1}(S_{via}/0.8g_{via})}{\varepsilon_{eff}} \quad (4)$$

An estimate of ε_{eff} is proposed by [18] and is used in this work to calculate α.

$$\varepsilon_{eff} = \frac{\varepsilon_r + 1}{2} - \frac{\varepsilon_r - 1}{2} \times \exp\left(\frac{-13h}{a}\right) - \left(\frac{-100h}{L_x} - 2g + 10h\right) \quad (5)$$

Similarly, capacitance occurs with the inductance obtained in (2). In [17] an empirical equation to estimate the total inductance was also proposed. This equation is shown below.

$$L_{eq} = \frac{L_v(N_{via} - 1)}{cosh^{-1}(1 + \beta)} \quad (6)$$

Where β is an adjustment factor for the mutual inductances that for this work was adapted from [17], from a wide set of parametric simulations using ANSYS HFSS. So, an equation of β that best meets the specifications of this work was achieved.

$$\beta = 21.5846 \ln(h/(2R_{via})) + 14.365 \quad (7)$$

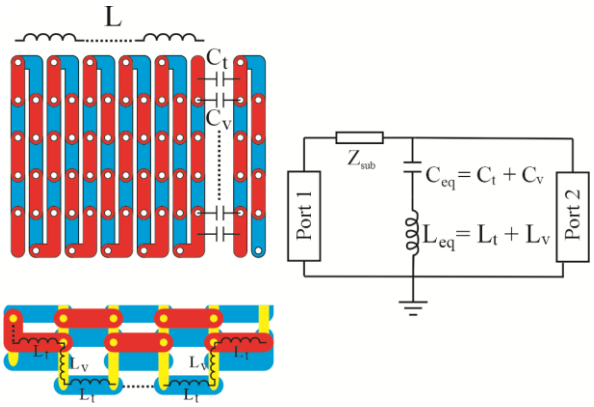

Fig. 6. Planar and 2.5D sections of FSS4 and their equivalent circuit.

According to (1) to (7), the equivalent circuits of the analyzed FSS were obtained, with the exception of the FSS1 which is totally planar and its equivalent circuit was obtained from simulations using ANSYS HFSS. The proposed model is valid for typical FSS dimensions. The inductance and capacitance values of the equivalent circuits can be seen in Table I.

Fig. 7 shows the comparison of the transmission coefficients simulated in ANSYS HFSS and by the ECM simulated in Advanced Design System (ADS). For all structures, the ECM method presents an excellent agreement with the HFSS results, thus proving that the equivalent circuit model proposed in this work is valid for the proposed structure.

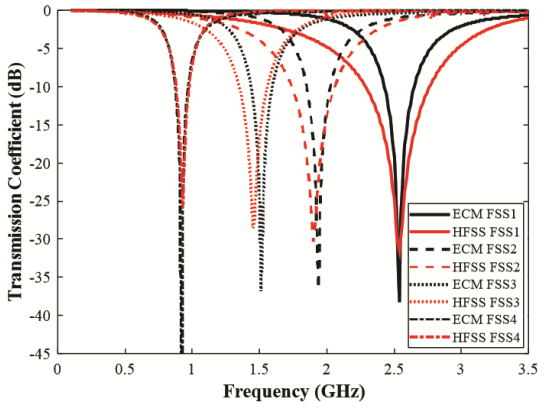

Fig. 7. FSS structures simulated transmission coefficient results in HFSS and ECM for FSS1 to FSS4 illustrated in Figs. 2(a) to 2(d), respectively.

V. Experimental Results

To evaluate the performance of the proposed 2.5D FSS (case 4), a prototype was fabricated and measured. The FSS prototype consists of an array of 20 x 20 elements, as shown in Fig. 8(a), printed on both sides of a FR-4 dielectric layer. The overall size of the FSS prototype is 200 mm x 200 mm.

The measurement setup consists basically of two A.H. Systems Inc.-SAS-571 horn antennas (a transmitting and a receiving), cables, and a Rohde & Schwarz-ZVB14 vector network analyzer (VNA), as shown in Fig. 8(b).

TABLE I
ECM PARAMETERS

Structures	L_{eq} (nH)	C_{eq} (pF)
FSS1	0.6580	5.9860
FSS2	0.8804	7.5053
FSS3	1.3183	8.3890
FSS4	2.1543	13.8940

Fig. 9 shows a comparison between measured and simulated results for the frequency behavior of the transmission coefficient, magnitude of S_{21}(dB), of the proposed 2.5D FSS with the array element shown in Fig. 2(d). The FSS simulated response in HFSS presented a resonance frequency at 920 MHz and a relative bandwidth of 12%, the simulation of ECM presented a resonance frequency at 920 MHz and a relative bandwidth of 12%, while the corresponding measured values are 910 MHz for the resonance frequency and 9% for the relative bandwidth.

Fig. 10 presents measurement results for different values of the electromagnetic wave incidence angle, θ. As in the simulation, the measured results show that the structure exhibits an excellent angular stability and the FSS resonant frequency results are about the same for incident angles up to 50°. Also, very good relative bandwidth results are observed, ensuring about the same FSS rejection band for incident angles up to 50°.

Table II summarizes the simulation and measurement results obtained for the proposed 2.5D FSS structure, showing a good agreement between simulation and measurement results.

Table III summarizes the results obtained for the FSS structure proposed in this work and those of FSS structures developed by other authors and available in the literature, for 900 MHz applications. Fields with a "-" are values not reported by the authors. The proposed 2.5D FSS presents a high performance with respect to the unit cell size miniaturization.

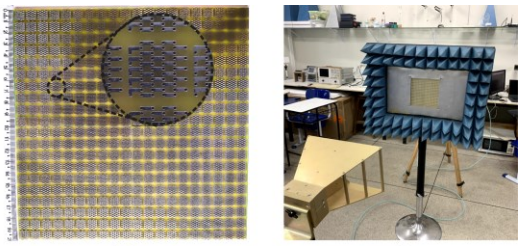

(a) (b)

Fig. 8. Photographs of the (a) 2.5D FSS prototype and (b) measurement setup

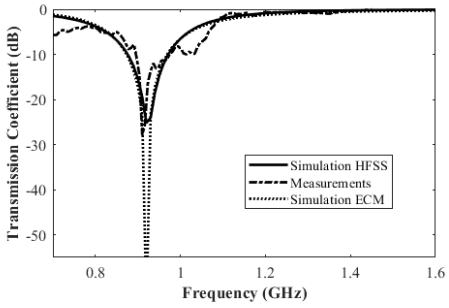

Fig. 9. Simulation and measurement results for the transmission coefficient, magnitude of S21 (dB), of the proposed 2.5D FSS.

TABLE II
PROPOSED FSS MEASURED AND HFSS SIMULATED RESULTS

θ	Frequency (GHz)		BW %	
	Simulation	Measurement	Simulation	Measurement
0	0.920	0.910	12.00	9.0
30°	0.930	0.923	12.22	8.9
50°	0.930	0.910	15.56	11.5

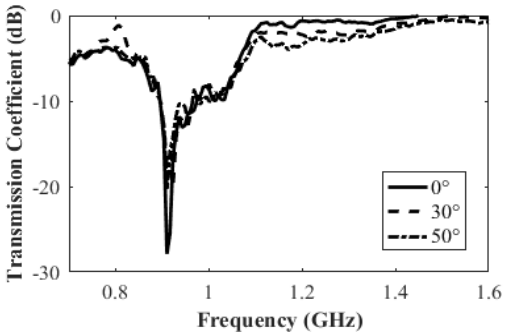

Fig. 10. Measurement results for the transmission coefficient, magnitude of S21 (dB), of the proposed 2.5D FSS, at different incident angle values.

TABLE III
MINIATURIZED AND ULTRAMINIATURIZED FSS STRUCTURES FOR 900 MHZ APPLICATIONS: UNIT CELL SIZE COMPARISON

Reference	FSS structure	Substrate dielectric constant, ε_r	BW %	Substrate thickness, h (mm)	Unit cell size
[12]	2.5D	2.2	10.1	2.0	$0.072\lambda_0 \times 0.072\lambda_0$
[19]	2D	1.8	-	-	$0.30\lambda_0 \times 0.30\lambda_0$
[20]	2D	4.3	28.6	1.6	$0.14\lambda_0 \times 0.14\lambda_0$
[21]	2D	2.2	19	1.57	$0.18\lambda_0 \times 0.18\lambda_0$
[22]	2D	3.4	10.8	0.5	$0.14\lambda_0 \times 0.14\lambda_0$
[23]	2D	4.4	-	1.0	$0.15\lambda_0 \times 0.15\lambda_0$
[24]	2D	2.2	-	0.1	$0.17\lambda_0 \times 0.17\lambda_0$
This work	2.5D	4.4	12	1.6	$0.03\lambda_0 \times 0.03\lambda_0$

VI. CONCLUSION

In this work, a 2.5D ultraminiaturized FSS band reject was proposed for the 900 MHz band. The scattering properties of several 2.5D FSS were investigated. An equivalent circuit model was proposed to analyze the proposed FSS structures. This model presented an excellent agreement when compared to the HFSS simulations and measurements, showing itself to be a fast and efficient method to calculate resonance frequency. The proposed FSS shows excellent angular stability for variations in the angle of incidence of the electromagnetic wave from 0° to 50°, for TE polarization. The unit cell size of the proposed FSS is $0.03\lambda_0$ x $0.03\lambda_0$, where λ_0 is the free space wavelength for the FSS resonant frequency. In comparison with the works of other authors, listed in Table II, the proposed 2.5D FSS presents a better performance with respect to the unit cell size miniaturization. In addition, a 2.5D FSS structure was fabricated and measured for comparison purpose. A good agreement was achieved between simulation and measurement results.

REFERENCES

[1] R. S. Anwar, L. Mao and H. Ning, "Frequency selective surfaces: A review," *Appl. Sci.,* 8, 1689, 2018, doi: 10.3390/app8091689.

[2] Q. Guo, Z. Li, J. Su, J. Song and L. Y. Yang, "Active frequency selective surface with wide reconfigurable passband," IEEE Access, vol. 7, pp. 38348-38355, 2019, doi: 10.1109/ACCESS.2019.2906219.

[3] L. Zhao et al., "An ultraminiaturized dual-stopband frequency selective surface for ultra high frequency," IEEE Access, vol. 8, pp. 44830-44835, 2020, doi: 10.1109/ACCESS.2020.2978217.

[4] P.-C. Zhao, Z. Zong, W. Wu, B. Li and D. Fang, "Miniaturized-element bandpass FSS by loading capacitive structures," *IEEE Trans. Antennas Propag.,* vol. 67, no. 5, pp. 3539-3544, May 2019, doi: 10.1109/TAP.2019.2902633.

[5] V. P. Silva Neto, M. J. Duarte and A. G. D'Assunção, "Full-wave analysis of stable cross fractal frequency selective surfaces using an iterative procedure based on wave concept," *Int. Journal Antennas Propag*., vol. 2015, Article ID 401210, 7p., 2015, doi: 10.1155/2015/401210.

[6] A. Gomes Neto, J. e Silva, I. Coutinho, M. Alencar, and D. de Andrade, "Triple Band Reject Frequency Selective Surface with Application to 2.4 GHz Band", *JCIS*, vol. 35, no. 1, pp. 77-85, Apr. 2020, doi: 10.14209/jcis.2020.8.

[7] U. Farooq, M. F. Shafique and M. J. Mughal, "Polarization insensitive dual band frequency selective surface for RF shielding through glass windows," *IEEE Trans. Electromagn. Compat.,* vol. 62, no. 1, pp. 93-100, Feb. 2020, doi: 10.1109/TEMC.2019.2893408.

[8] T. Cheng, Z. Jia, T. Hong, W. Jiang and S. Gong, "Dual-band frequency selective surface with compact dimension and low frequency ratio," IEEE Access, vol. 8, pp. 185399-185404, 2020, doi: 10.1109/ACCESS.2020.3030131.

[9] S. Habib, G. I. Kiani and M. F. U. Butt, "A convoluted frequency selective surface for wideband communication applications," IEEE Access, vol. 7, pp. 65075-65082, 2019, doi: 10.1109/ACCESS.2019.2916882.

[10] V. P. Silva Neto, A. G. D'Assunção and H. Baudrand, "Analysis of finite size nonuniform stable and multiband FSS using a generalization of the WCIP method," *IEEE Trans. Electromagn. Compatib.,* vol. 60, no. 6, pp. 1802-1810, Dec. 2018, doi: 10.1109/TEMC.2017.2785787.

[11] W. Wang, Q. Cao and Y. Zheng, "Bandstop frequency-selective structures based on stepped-impedance loop resonators: design, analysis, and measurement," *IEEE Trans. Antennas Propag.*, vol. 67, no. 2, pp. 1053-1064, Feb. 2019, doi: 10.1109/TAP.2018.2880011.

[12] W. Yin, H. Zhang, T. Zhong and X. Min, "A novel compact dual-band frequency selective surface for GSM shielding by utilizing a 2.5-dimensional structure," *IEEE Trans. Electromagn. Compat.,* vol. 60, no. 6, pp. 2057-2060, Dec. 2018, doi: 10.1109/TEMC.2018.2790584.

[13] W. Yin, H. Zhang, T. Zhong and X. Min, "Ultra-miniaturized low-profile angularly-stable frequency selective surface design," *IEEE Trans. Electromagn. Compat.,* vol. 61, no. 4, pp. 1234-1238, Aug. 2019, doi: 10.1109/TEMC.2018.2881161.

[14] P.-S. Wei, C.-N. Chiu and T.-L. Wu, "Design and analysis of an ultraminiaturized frequency selective surface with two arbitrary stopbands," *IEEE Trans. Electromagn. Compat.,* vol. 61, no. 5, pp. 1447-1456, Oct. 2019, doi: 10.1109/TEMC.2018.2864546.

[15] L. Qiao, Z. Zheng, W. Cui and L. Wang, "A survey on Wi-Fi HaLow technology for internet of things," *2018 2nd IEEE Conference on Energy Internet and Energy System Integration (EI2)*, Beijing, 2018, pp. 1-5, doi:.

[16] N. N. Rao, *Elements of engineering electromagnetics*. Prentice Hall, NJ, USA, 2004.

[17] T. Hussain, Q. Cao, J. K. Kayani and I. Majid, "Miniaturization of frequency selective surfaces using 2.5-D knitted structures: design and synthesis," *IEEE Trans. Antennas Propag.*, vol. 65, no. 5, pp. 2405-2412, May 2017, doi: 10.1109/TAP.2017.2673809.

[18] D. Ferreira, R. F. Caldeirinha, I. Cuinas, and T. R. Fernandes, "Square loop and slot frequency selective surfaces study for equivalent circuit model optimization," *IEEE Trans. Antennas Propag*., vol. 63, no. 9, pp. 3947–3955, 2015, doi: 10.1109/TAP.2015.2444420.

[19] W. Kiermeier and E. Biebl, "New dual-band frequency selective surfaces for GSM frequency shielding," 2007 European Microwave Conference, Munich, 2007, pp. 222-225, doi: 10.1109/EUMC.2007.4405166.

[20] F. C. Seman and N. K. Khalid, "Investigations on fractal square loop FSS at oblique incidence for GSM applications," 2014 Electrical Power, Electronics, Communicatons, Control and Informatics Seminar (EECCIS), Malang, 2014, pp. 62-66, doi: 10.1109/EECCIS.2014.7003720.

[21] M. M. Masud, B. Ijaz, I. Ullah and B. Braaten, "A compact dual-band EMI metasurface shield with an actively tunable polarized lower band," *IEEE Trans. Electromagn. Compat.,* vol. 54, no. 5, pp. 1182-1185, Oct. 2012, doi: 10.1109/TEMC.2012.2210899.

[22] R. Sivasamy, L. Murugasamy, M. Kanagasabai, E. F. Sundarsingh and M. G. N. Alsath, "A low-profile paper substrate-based dual-band FSS for GSM shielding," *IEEE Trans. Electromagn. Compat.,* vol. 58, no. 2, pp. 611-614, Apr. 2016, doi: 10.1109/TEMC.2015.2498398.

[23] M. Kartal, J. J. Golezani and B. Doken, "A triple band frequency selective surface design for GSM systems by utilizing a novel synthetic resonator," *IEEE Trans. Antennas Propag.,* vol. 65, no. 5, pp. 2724-2727, May 2017, doi: 10.1109/TAP.2017.2670230.

[24] L. B. Wang, K. Y. See, B. Salam, A. C. W. Lu, J. W. Zhang and S. Tengiz, "Tri-band frequency selective band-stop shield using screen printing technique," 2012 Asia-Pacific Symp. Electromagnetic Compatibility, Singapore, 2012, pp. 661-664, doi: 10.1109/APEMC.2012.6237795.